Classification of internal solitary wave breaking over a slope

Keisuke Nakayama,[1] Takahiro Sato,[1] Kenji Shimizu,[1] and Leon Boegman[2]
[1]*Department of Civil Engineering, Kobe University, 1-1 Rokkodai-Cho, Nada-Ku, Kobe-Shi, Kobe 657-0013, Japan*
[2]*Environmental Fluid Dynamics Laboratory, Department of Civil Engineering, Queen's University, 58 University Avenue, Kingston, Ontario K7L 3N6, Canada*

(Received 11 August 2018; published 2 January 2019)

Breaking of shoaling internal solitary waves (ISWs) is important for mixing and mass transport processes in oceans and lakes. For ISWs in a two-layer stratified fluid, previous studies identified four breaker types: surging, plunging, collapsing, and fission. The latest classification of these breaker types is based on the wave slope S_w and the bottom slope S; however, this classification was found to be unsatisfactory in delineating collapsing and plunging breakers. The present study proposes a new classification for these two breaker types using extended data sets, consisting of published experimental data and the results of new numerical simulations. It was found that a single nondimensional index $B_{\mathrm{ISW}} = (S/S_w)\mathrm{Re}_{\mathrm{ISW}}{}^2$ delineates collapsing and plunging breakers in the extended data, where $\mathrm{Re}_{\mathrm{ISW}}$ is a new wave Reynolds number that accounts for nonlinear wave steepening.

DOI: 10.1103/PhysRevFluids.4.014801

I. INTRODUCTION

Breaking of shoaling internal waves is an important cause of mixing and diapycnal mass transport in oceans [1] and lakes [2–4]. For example, several large-wave shoaling events per tidal cycle may supply sufficient nutrients to the photic zone [5] or create a surface patch with high phytoplankton concentration [6]. Internal-wave breaking can also induce residual currents and associated diapycnal mass transport, as observed in laboratory-scale experiments [7–9], in lakes [10], in estuaries [11,12], and on continental shelves [13]. Breaking of internal solitary waves (ISWs) is also considered to be important for sediment transport and resuspension [12,14–16]. Shoaling ISWs can break in various ways and knowing which type of ISW breaking occurs is essential for understanding the ensuing mass transport [15] and energetics [17,18]. In this study, we propose to extend the latest classification of ISW breaking in a two-layer stratified fluid [19] by introducing Reynolds number effects.

ISWs have an unchanged form as they propagate in deep water, but they deform and ultimately break over sloping topography in relatively shallow water, such as on continental shelves. One of the important parameters characterizing the deformation is the turning point, where the pycnocline is at mid depth, and the polarity of an ISW changes from a wave of depression in deeper water to that of elevation in shallower water [20,21]. If the bottom slope is mild enough to allow "adiabatic" adjustment to the changing water depth, an incoming ISW of depression may transform into a packet of ISWs [22]; this process is called fission. ISWs resulting from fission are predominantly waves of elevation because fission occurs upslope from the turning point [19]. If the bottom slope is sufficiently steep that an incident ISW does not have sufficient time for adiabatic adjustment, the trailing face of the ISW steepens. Subsequently, if the wave has sufficient time to steepen before reaching the turning point, the trailing face plunges, or overturns in the upslope direction [23]; however, if the incoming wave does not have sufficient time to overturn, the trailing face surges upslope. These types of ISW breaking are called plunging and surging, respectively (see Aghsaee *et al.* [19])

In addition to fission, plunging, and surging, ISWs may break due to instability. Shear instability may occur when the Richardson number $\mathrm{Ri} = N^2/{u_z}^2$ (N is the buoyancy frequency and u_z is the vertical shear) becomes sufficiently low [24–26]. This process is important in relatively deep water but does not appear to be so over a slope in relatively shallow water [20,27]. Another type of instability occurs when the adverse pressure gradient induced by an ISW causes separation of the bottom boundary layer and the shed vortices destabilize the pycnocline [28–31]. This process becomes more important for shoaling ISWs because the adverse pressure gradient increases as the wave trough approaches the bottom [32]; this type of ISW breaking is called collapsing.

Breaking of an ISW can create a train of ISWs of elevation with trapped cores, which have closed streamlines when seen in a reference frame moving with the propagation speed [18,33]. Such ISWs are often referred to as boluses [34,35]. They are known to occur after collapsing [34,35] and surging [19]. Boluses have important implications for mass transport because they can have trapped cores that carry mass upslope through the pycnocline [36,37]. Although we did not investigate boluses in this study, the dependence of bolus formation on ISW breaker types illustrates the importance of ISW classification.

Previous studies suggested several classifications of ISW breaking. Boegman *et al.* [38] (hereafter, BG) introduced an internal Iribarren number by modifying the Iribarren number originally proposed for surface waves [39–42], and classified spilling, plunging, and collapsing breakers in their laboratory experiments. (Note, however, that the classification of spilling breaker is now considered to be erroneous [19].) Aghsaee *et al.* [19] (hereafter, AG) later introduced four types of ISW breaking: fission, collapsing, plunging, and surging. They showed that the internal Iribarren number alone is insufficient to classify these types of breaking, and proposed two-parameter classification based on the wave slope S_w and the bottom slope S. However, this classification did not satisfactorily delineate plunging and collapsing breakers in the laboratory experiments by BG and in the numerical experiments conducted in this study. The laboratory experiments by Sutherland *et al.* [43] also showed that S_w and S did not delineate plunging and collapsing breakers [see their Fig. 9(a)], but they were unable to propose alternative classification for these breakers.

This study aims to extend the previous classification of AG by introducing Reynolds number effects that delineates plunging and collapsing breakers. Following AG, we focused on ISWs in a two-layer stratified fluid propagating into quiescent water and shoaling over a uniform slope. We conducted numerical experiments of ISW breaking, but extended the work of AG by allowing the density difference between the layers to vary. The simulation results were analyzed, together with previous laboratory [38] and numerical [19] experiments, to derive a new parameter to classify plunging and collapsing breakers.

II. METHODS

A. Present numerical experiments

In this study, a three-dimensional non-hydrostatic model, Fantom3D, was used to analyze the breaking of shoaling ISWs. Fantom3D is an object-oriented parallel computing model for the analysis of environmental fluid dynamics [44–47], based on the Reynolds-averaged Navier-Stokes (RANS) equations in the height (z) coordinate. A free surface was applied to the top boundary, and a no-slip and slip conditions were given on the bottom and lateral boundaries, respectively. The partial cell scheme [48] was used to represent a uniform bottom slope in the z-coordinate model.

Sub-grid-scale turbulence was parameterized with a k-ε turbulence closure scheme [49,50] to account for turbulent mixing and dissipation after ISW breaking; however, the turbulence parameterization is not important for the purpose of this study because, as shown later, processes up to (but not after) the point of wave breaking are laminar in the laboratory-scale problems considered in this study [51].

Both energy reflection and breaker type are determined during the initial two-dimensional wave/slope interaction occurring at large scale [19,52]. Therefore, the computational domain was two-dimensional (2D), consisting of an open boundary, a flat-bottom section, and a uniform-slope

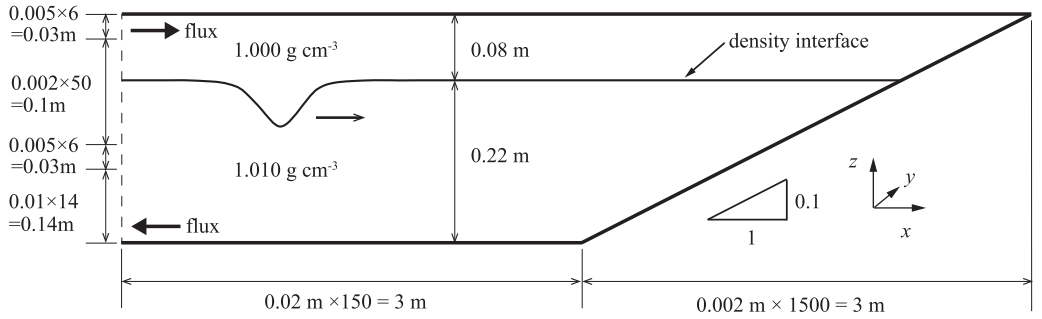

FIG. 1. Schematic diagram of computational domain and mesh size. This figure indicates case 3 in Table I.

section (Fig. 1). The length of the flat-bottom section before the toe of the slope was 3.0 m, and the total water depth H was 0.3 m for all cases. The bottom slope S, in the uniform-slope section, varied from 0.03 to 0.3, to be consistent with AG. The size of the computational mesh was 0.002 m × 0.002 m in the wave breaking region over the slope and coarser elsewhere for all the cases.

We applied an initial hyperbolic tangent stratification:

$$\rho(z) = \rho_1 + \frac{\Delta\rho}{2}\left(1 - \tanh\frac{z + h_1}{0.5a}\right), \tag{1}$$

where z is the upward-positive vertical coordinate with origin at equilibrium water surface, h_1 is the upper-layer thickness, ρ_1 is the density of the upper layer, $\Delta\rho$ is the density difference between the upper and lower layers, and a (=0.01 m) is the thickness of the density interface. We used upper-layer thicknesses ranging from $h_1 = 0.04$ m to 0.08 m. To investigate the influence of the specific density ratio $\varepsilon_d[=\Delta\rho/(\rho_1 + \Delta\rho)]$, we considered 17 cases with a lower-layer density $\rho_2 = 1010\,\mathrm{kg\,m^{-3}}$, 4 cases with $\rho_2 = 1020\,\mathrm{kg\,m^{-3}}$, 7 cases with $\rho_2 = 1040\,\mathrm{kg\,m^{-3}}$, and 1 case with $\rho_2 = 1080\,\mathrm{kg\,m^{-3}}$, while holding an upper-layer density at $\rho_1 = 1000\,\mathrm{kg\,m^{-3}}$ (Table I). In comparison, AG and BG used $\varepsilon_d = 0.04$ and 0.02, respectively. The model was forced at the open boundary using the third-order ISW solution [53,54]. The ISW amplitude A was varied from 0.013 m to 0.049 m in order to investigate four different breaker types (Table I). The results from the present numerical experiments are denoted as "NS". The thickness of the density interface may control internal wave breaking in a two-layer stratification; however, we consider the thin density interface case following Boegman *et al.* [38] and Aghsaee *et al.* [19] with a quasi-two-layer system. Sutherland *et al.* [43] performed experiments on breaker classification with varying interfacial thickness, but only report results from experiments with a thin interface, thereby suggesting those with a thick interface are inappropriate for the present investigation. The effect of the interfacial thickness on the type of breaking remains to be investigated elsewhere.

B. Previous laboratory and numerical experiments

In addition to the numerical experiments described above, we included numerical experiments by AG and the laboratory experiments by BG, to find a more universal classification of ISW breakers. AG investigated breaking criteria using 2D direct numerical simulations. They defined four breaker types, fission, collapsing, plunging, and surging, but also found mixed-mode breaker types, such as collapsing-surging and collapsing-plunging breakers. In AG, the total water depth H was 0.15 m, and the upper-layer thickness h_1 ranged from 0.02 m to 0.06 m, with a specific density ratio ε_d of 0.04. They examined 7 different slope gradients S from 0.01 to 0.3. The initial condition was given using the Dubreil–Jacotin–Long (DJL) equation [33].

BG carried out laboratory experiments in a tilting tank. They investigated breaking of high-frequency internal waves over a uniform slope, formed by the degeneration of an internal basin-scale

TABLE I. Main parameters from numerical experiments conducted in this study. Note that $\rho_1 = 1.00\,\mathrm{g\,cm^{-3}}$ for all the cases. U is the estimate of maximum free-stream current speed outside of the bottom boundary layer, and c is the propagation speed of the leading incident ISW.

	ρ_2(g cm^{-3})	$h1$ (m)	$h2$ (m)	A (m)	λ(m)	U(ms^{-1})	c(ms^{-1})	S	Breaker type
Case 1	1.04	0.08	0.22	0.0278	0.900	0.0233	0.166	0.03	fission
Case 2	1.01	0.08	0.22	0.0490	0.873	0.0240	0.086	0.1	plunging
Case 3	1.01	0.08	0.22	0.0375	0.889	0.0172	0.085	0.1	plunging
Case 4	1.01	0.08	0.22	0.0489	0.896	0.0240	0.086	0.067	plunging
Case 5	1.01	0.08	0.22	0.0638	1.057	0.0360	0.087	0.067	plunging
Case 6	1.01	0.08	0.22	0.0213	0.961	0.0087	0.081	0.1	collapsing-plunging
Case 7	1.01	0.08	0.22	0.0128	1.105	0.0050	0.080	0.1	collapsing
Case 8	1.01	0.08	0.22	0.0255	0.908	0.0107	0.083	0.3	surging
Case 9	1.02	0.08	0.22	0.0317	0.906	0.0195	0.117	0.03	fission
Case 10	1.02	0.08	0.22	0.0318	0.903	0.0195	0.117	0.1	collapsing-plunging
Case 11	1.01	0.08	0.22	0.0199	0.973	0.0081	0.082	0.03	fission
Case 12	1.01	0.08	0.22	0.0199	0.971	0.0081	0.080	0.05	fission
Case 13	1.01	0.08	0.22	0.0199	0.970	0.0081	0.082	0.1	collapsing-plunging
Case 14	1.01	0.08	0.22	0.0199	0.968	0.0081	0.080	0.2	surging
Case 15	1.04	0.06	0.24	0.0190	0.691	0.0122	0.150	0.06	fission
Case 16	1.01	0.06	0.24	0.0187	0.699	0.0060	0.075	0.06	collapsing
Case 17	1.04	0.08	0.22	0.0379	0.862	0.0344	0.169	0.1	plunging
Case 18	1.08	0.08	0.22	0.0378	0.844	0.0483	0.240	0.1	plunging
Case 19	1.04	0.08	0.22	0.0214	0.992	0.0172	0.164	0.1	collapsing-plunging
Case 20	1.01	0.08	0.22	0.0213	0.965	0.0087	0.083	0.1	collapsing-plunging
Case 21	1.04	0.06	0.24	0.0363	0.593	0.0262	0.158	0.08	plunging
Case 22	1.04	0.06	0.24	0.0298	0.624	0.0204	0.160	0.15	plunging
Case 23	1.04	0.06	0.24	0.0152	0.722	0.0095	0.147	0.2	surging
Case 24	1.01	0.06	0.24	0.0150	0.727	0.0047	0.075	0.2	surging
Case 25	1.02	0.06	0.24	0.0158	0.757	0.0070	0.106	0.15	surging
Case 26	1.01	0.06	0.24	0.0157	0.761	0.0050	0.075	0.15	surging
Case 27	1.02	0.04	0.26	0.0216	0.461	0.0071	0.094	0.075	collapsing
Case 28	1.01	0.05	0.25	0.0266	0.559	0.0078	0.073	0.06	collapsing
Case 29	1.01	0.06	0.24	0.0128	0.801	0.0040	0.075	0.1	collapsing

seiche. The total water depth H and the specific density ratio ε_d were 0.29 m and 0.02, respectively. They varied the upper-layer thickness h_1 from $\approx$0.06 m to $\approx$0.085 m, and used two slope gradients, $S = 0.0967$ and 0.145. Since it is possible that wave breaking occurred before ISWs were fully developed through the degeneration process in the experiments, we investigated whether the leading high-frequency internal wave, in each experimental case, can be considered as an ISW (see Appendix). From this analysis, we used six cases in which the leading incident wave approximately satisfied the theoretical amplitude–wavelength relationship for an ISW [Table II and Fig. 8].

C. Analytical methods

We develop a new classification of ISW breaker types using parameters that depend on the background conditions (e.g., bottom slope and stratification) and the incident wave, but not the wave as it deformed over the slope. This strategy was consistent with the classification of ISW breakers by AG, which was based on the bottom slope S and the wave slope $S_w = A/\lambda$. Here, A is the incident-wave amplitude, and λ is the incident-wave wavelength defined as

$$\lambda = \frac{\int_{-\infty}^{+\infty} \eta(x)dx}{A}, \tag{2}$$

TABLE II. Main parameters from laboratory experiments by Boegman *et al.* [38]. Only cases that approximately satisfy theoretical amplitude-wavelength scale relationship of internal solitary waves are chosen (see Fig. 8). Wavelengths are slightly adjusted to satisfy the theoretical amplitude-wavelength scale relationship.

	ρ_2 (gcm^{-3})	$h_1(m)$	h_2(m)	A (m)	λ(m)	S	Breaker type
Case B1	1.02	0.06	0.23	0.0256	0.674	0.145	plunging
Case B2	1.02	0.058	0.232	0.0068	0.955	0.145	collapsing
Case B3	1.02	0.087	0.203	0.0244	1.056	0.097	plunging
Case B4	1.02	0.087	0.203	0.0245	1.056	0.097	plunging
Case B5	1.02	0.083	0.207	0.0407	1.066	0.145	plunging
Case B6	1.02	0.083	0.207	0.0374	1.032	0.145	plunging

and η is the downward interface displacement [55]. These parameters may be combined into the internal Iribarren number, $\xi_i = S/S_w{}^{0.5}$. We used different wave Reynolds numbers as parameters representing boundary-layer separation. Diamessis and Redekopp [30] and Boegman and Ivey [15] introduced the following wave Reynolds numbers

$$\mathrm{Re} = \frac{c_0 H}{\nu}, \tag{3}$$

$$\mathrm{Re}_w = \frac{c_0 A}{\nu}, \tag{4}$$

respectively. Here, $H = h_1 + h_2$ is the total depth, ν is the kinematic viscosity or eddy viscosity before boundary-layer separation, c_0 is the propagation speed of long linear waves over a flat bottom,

$$c_0 = \sqrt{\varepsilon g \frac{h_1 h_2}{H}}, \tag{5}$$

and g is the gravitational acceleration. Aghsaee *et al.* [32] introduced the momentum-thickness Reynolds number to provide a criterion for the separation of a laminar boundary layer over a flat bottom; however, we did not consider this in the present study with waves shoaling over a sloping bed.

The "critical depth" is defined as the position where the total water depth is divided with the ratio of ${\rho_1}^{0.5}$ and ${\rho_2}^{0.5}$ from water surface. It is easily found from the Korteweg–de Vries (KdV) theory that an ISW is convex toward the critical depth (Fig. 2). Therefore, there exists a "turning point" where an incoming ISW changes the polarity from a wave of depression in deeper water to a wave of elevation in shallower water. Nakayama *et al.* [9] defined the horizontal length from the turning point to the slope–interface intersection at equilibrium as the critical length L_C. They summarized that L_C should be taken into account in order to clarify how internal waves are excited and how residual currents are driven over a slope when a collapsing breaker occurs. For a plunging ISW breaker, AG found that the breaking point occurs offshore from a turning point. We define the horizontal length from the toe of the slope to the turning point as the critical slope length L_{SC}.

To check whether the bottom boundary layer under an ISW was laminar before breaking, we considered a Reynolds number for boundary layer flows under a solitary wave

$$\mathrm{Re}_{\mathrm{BL}} = \frac{aU}{\nu}, \tag{6}$$

where U is the maximum free-stream current speed in the lower layer, and $a \sim (2c_0)^{-1}\lambda U$ is half the wave-induced horizontal water-particle displacement in the free-stream region [56]. Previous laboratory [56] and numerical [57,58] experiments showed that the laminar-turbulent transition occurs when $\mathrm{Re}_{\mathrm{BL}} = O(10^5)$.

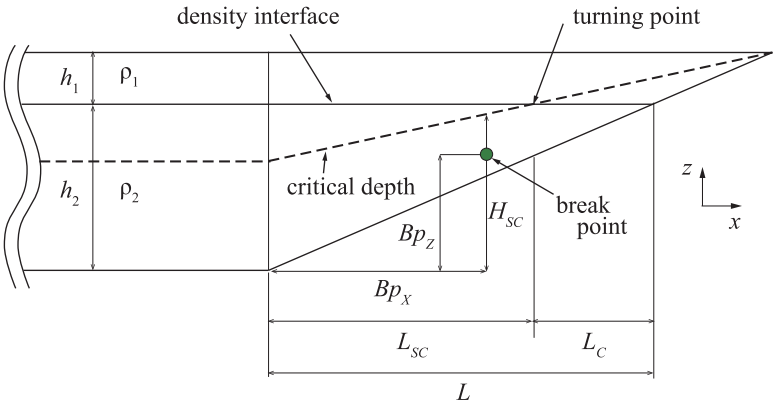

FIG. 2. Definition of critical slope length, L_{SC}, and critical length, L_C, and breaking points, Bp_X and Bp_Z.

To investigate the characteristics of the breaking point for various ISW breakers, the location of the breaking point was estimated to be the location where the vertical pressure gradient becomes zero [9]:

$$\frac{\partial p}{\partial z} = 0 \quad \text{at density interface.} \tag{7}$$

This method enables precise detection of the breaking point, even if there is no distinguishable mixing of the density interface. The horizontal length between the toe of the slope to the breaking point is defined as Bp_X, the vertical length between the flat bottom to the breaking point is Bp_Z, and the vertical length between the flat bottom and the critical depth is H_{SC} (Fig. 2).

III. RESULTS

A. Present numerical experiments

As in AG, four different types of ISW breaker—fission, collapsing, plunging, and surging—were found to occur in our numerical experiments. Typical cases of fission (case 1), collapsing (case 7), plunging (case 3), and surging (case 8) are shown in Fig. 3. For fission, it was confirmed that an ISW with a longer wavelength was deformed into ISWs of elevation with shorter wavelengths that eventually broke over the slope [Fig. 3(a)]. As well known from previous studies, collapsing breakers induced a backward overturn of the interface near the front [i.e., anticlockwise overturn in Fig. 3(b)]. Plunging breakers showed a dynamic forward overturn along the trailing face [clockwise overturn in Fig. 3(c)]. For surging breakers, mixing occurred adjacent to the slope and the front ran-up over the slope, without major overturning of the density interface [Fig. 3(d)].

To investigate the influence of the turning point location on the breaker type, Bp_X/L_{SC} and Bp_Z/H_{SC} are plotted in Fig. 4. The breaking points for plunging occurred downslope from the turning point [19]. In contrast, the breaking points for surging, collapsing, and fission were likely to occur upslope from the turning point. The vertical location of breaking was found to occur below the critical depth and the breakers were all located at almost the same height. Mixed-mode breakers (collapsing-plunging and collapsing-surging breakers) are not shown in Fig. 4.

In all the present numerical experiments, the bottom boundary layer flows before ISW breaking were laminar, $\mathrm{Re_{BL}} = O(10^3)$, and well below the transition at $\mathrm{Re_{BL}} = O(10^5)$. For example, $U = O(10^{-2}\,\mathrm{m\,s^{-1}})$, $c_0 = O(0.1\,\mathrm{m\,s^{-1}})$, $\lambda = O(1\,\mathrm{m})$, and $\nu = 10^{-6}\,\mathrm{m\,s^{-1}}$ (Table I). We also confirmed that the use of molecular kinematic viscosity ($10^{-6}\,\mathrm{m^2\,s^{-1}}$) and the k-ε turbulence closure scheme gave essentially the same results before wave breaking. The above scaling arguments are also applicable to the experiments in AG and BG, and so the bottom boundary layer flows, from the previously published data, are hereafter considered to be laminar.

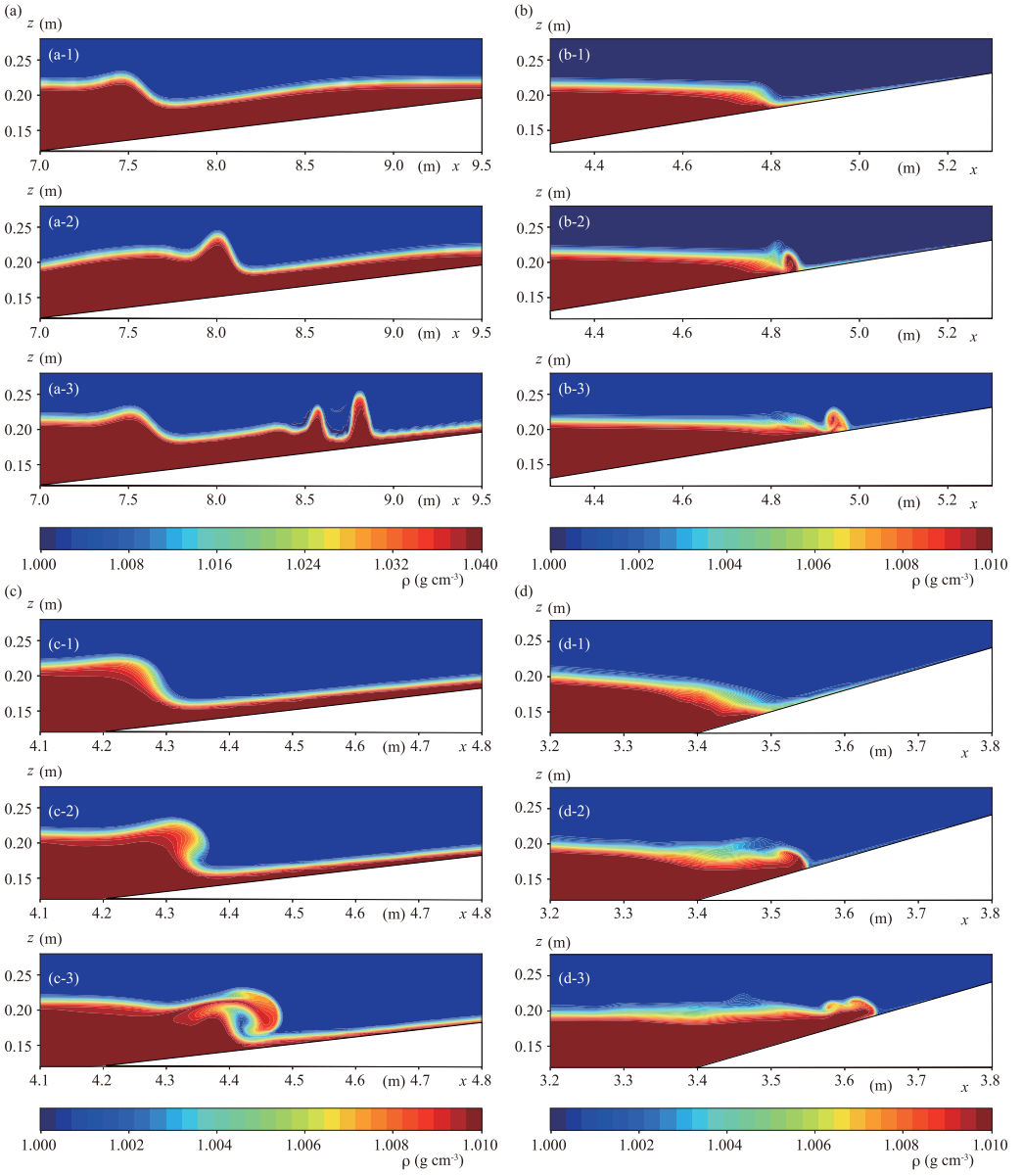

FIG. 3. Typical cases of different breaker types. (a) Fission (case 1 in Table I). (b) Collapsing (case 7 in Table I). (c) Plunging (case 3 in Table I). (d) Surging (case 8 in Table I). Contours indicate density.

B. Revisiting previous breaker classifications

Our numerical experiments and the laboratory experiments by BG showed that the breaker type could not be classified by using the internal Iribarren number (ξ_i), but surging and fission could be classified using S_w and S. In particular, we found that the criterion for a surging breaker by AG,

$$S > 7S_w, \tag{8}$$

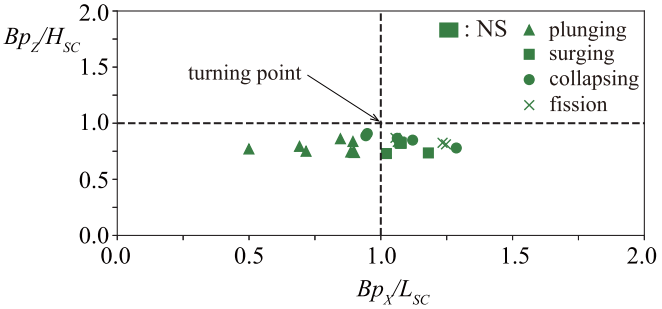

FIG. 4. Relationship between Bp_X/L_{SC} and Bp_Z/H_{SC}. All points are from NS. Triangles, squares, circles, and crosses indicate plunging, surging, collapsing, and fission, respectively.

holds for our extended data sets, except one laboratory case from BG (Fig. 5). However, as found by Sutherland *et al.* [43], plunging and collapsing breakers could not be separated using S_w and S in previously published data.

C. New breaker classification

We confirmed that surging breakers and fission could be classified using S_w and S, but it remains necessary to find a new parameter for classifying plunging and collapsing breakers. We attempted to use a wave Reynolds number to classify these breakers, because wave Reynolds number controls boundary-layer separation over a flat bottom [15,30–32]. Figures 6(a) and 6(b) show collapsing and plunging breakers as a function of (S/S_w) and Re or Re_w. Although (S/S_w) and Re do not delineate the two breaker types, (S/S_w) and Re_w do delineate them. However, the classification in Fig. 6(b) is not ideal because it requires two parameters [i.e., two lines in Fig. 6(b)].

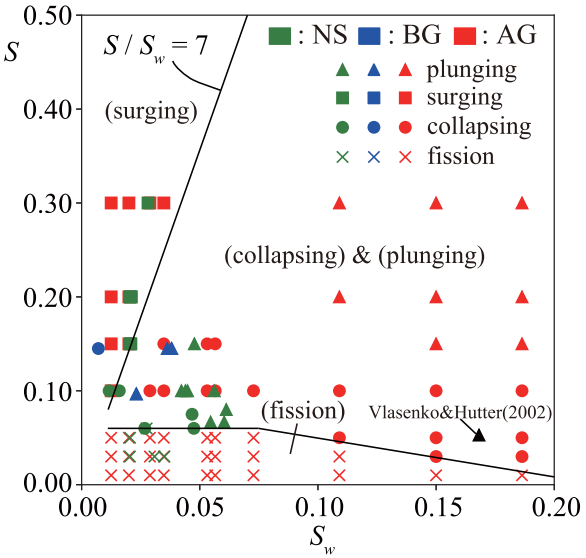

FIG. 5. ISW breaker types as a function of wave slope S_w and slope gradient S. Green, blue and red show NS, BG and AG, respectively. Triangles, squares, circles, and crosses indicate plunging, surging, collapsing, and fission, respectively.

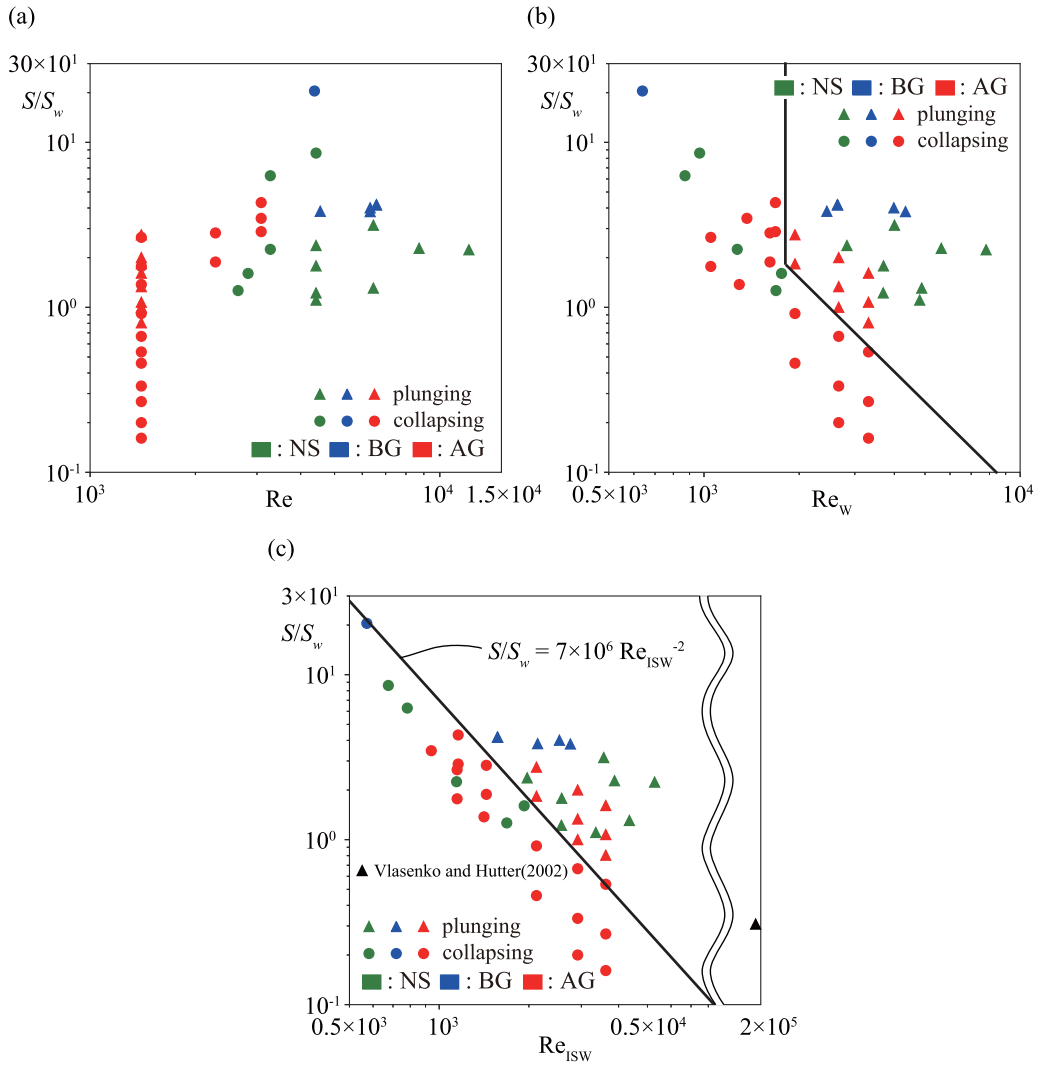

FIG. 6. ISW breaker types as functions of S/S_w and different wave Reynolds numbers. (a) Re, (b) Re_w, and (c) $\mathrm{Re}_{\mathrm{ISW}}$. Green, blue, and red show NS, BG, and AG, respectively. Triangles and circles indicate plunging and collapsing, respectively. Panel (c) shows proposed classification with solid line indicating the threshold between plunging and collapsing breakers.

To derive a single parameter that delineates collapsing and plunging breakers, we modified Re_w by considering wave steepening effects. We did so because a plunging breaker is not expected to occur when nonlinear wave steepening occurs relatively slowly, but Re_w does not capture such effects. For example, laboratory experiments in Nakayama *et al.* [8] showed only collapsing breakers when the upper- and lower-layer thicknesses were equal (note, however, that the incident waves were sinusoidal, not ISWs, in their experiments). Therefore, it appeared reasonable to use the increase in wave propagation speed, due to nonlinear effects αA, as a velocity scale to modify Re_w. Here, α is the coefficient of the nonlinear term in the KdV equation, defined as

$$\alpha = \frac{3}{2}\frac{c_0}{h_1 h_2}\frac{\rho_1 {h_2}^2 - \rho_2 {h_1}^2}{\rho_1 h_2 + \rho_2 h_1}. \tag{9}$$

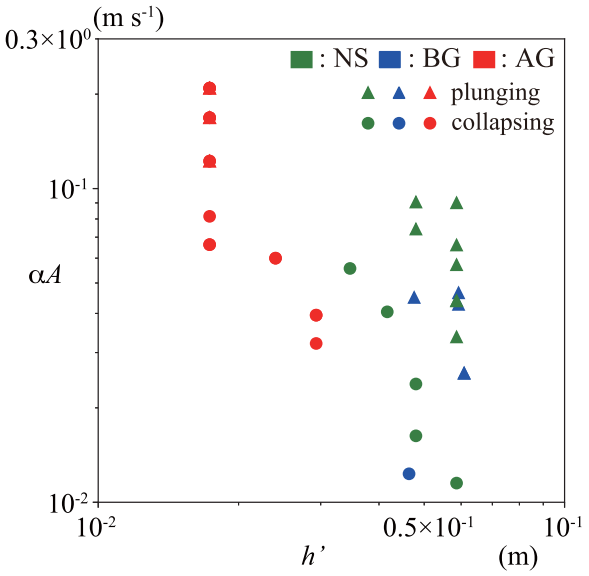

FIG. 7. ISW breaker types as a function of h' and αA. Green, blue, and red show NS, BG, and AG, respectively. Triangles and circles indicate plunging and collapsing, respectively.

We choose the following length scale to define a Reynolds number:

$$h' = \frac{h_1 h_2}{h_1 + h_2}. \tag{10}$$

Although α and h' change with water depth, the values in the flat-bottom section are used in the above expression because we aim to develop a classification based on incident-wave parameters. Figure 7 shows that the larger αA and h' become, the greater the tendency is toward plunging breakers, although some of the data points for plunging and collapsing breakers overlap because of the dependence on (S/S_w). Based on the above arguments, we propose the following wave Reynolds number:

$$\mathrm{Re}_{\mathrm{ISW}} \equiv \frac{\alpha A h'}{\nu}. \tag{11}$$

Figure 6(c) shows that collapsing and plunging breakers can be delineated by a straight line because it is found from Fig. 6(c) that the smaller the value of α is given, the more the greater tendency toward collapsing breakers. Therefore, $\mathrm{Re}_{\mathrm{ISW}}$ is revealed to have more universal application compared to Re_w. From the results in Fig. 6(c), we propose the following nondimensional index as a threshold between collapsing and plunging breakers:

$$B_{\mathrm{ISW}} \equiv (S/S_w)\mathrm{Re}_{\mathrm{ISW}}^2 \begin{cases} > 7 \times 10^6 & \text{plunging} \\ < 7 \times 10^6 & \text{collapsing.} \end{cases} \tag{12}$$

The meaning of B_{ISW} can also be understood from geometrical relationships, rather than the KdV theory. Because the specific density ratio between the upper and lower layers is small ($\varepsilon_d \ll 1$), α and L_{SC} can be written as

$$\alpha \sim \frac{3}{2} c_0 \frac{h_2 - h_1}{h_1 h_2}, \tag{13}$$

$$L_{\mathrm{SC}} \sim \frac{h_2 - h_1}{S}. \tag{14}$$

These expressions can be used to rewrite $\mathrm{Re}_{\mathrm{ISW}}$ as

$$\mathrm{Re}_{\mathrm{ISW}} \sim \frac{3}{2}\frac{L_{SC}S}{H}\mathrm{Re}_w, \tag{15}$$

which shows the importance of the critical slope length L_{SC}, the relationship between Re_w and $\mathrm{Re}_{\mathrm{ISW}}$ and the relationship between α and $(L_{\mathrm{SC}}S\,c_0/H)$. When a density interface is located close to the critical depth (L_{SC} tends to zero), $\mathrm{Re}_{\mathrm{ISW}}$ becomes smaller and collapsing breakers predominate, even if Re_w is relatively large.

An approximate (first-order) critical amplitude A_C, which delineates collapsing and plunging breakers, can be obtained from Eqs. (12) and (15) assuming the wavelength of the classical (first-order) KdV soliton, yielding

$$A_C \sim \frac{B_{\mathrm{ISW},C}^2}{27S^2\mathrm{Re}^4}\left(\frac{H^2}{h_1h_2}\right)^2\left(\frac{H}{L_{\mathrm{SC}}S}\right)^3, \tag{16}$$

where $B_{\mathrm{ISW},C}$ $(=7\times10^6)$ is the threshold between collapsing and plunging breakers. When L_{SC} becomes larger, the critical amplitude becomes smaller, which means that a plunging breaker is more likely to occur. It should be noted that the critical amplitude A_C is likely to be overestimated since the wavelength is underestimated by the first-order KdV theory [59].

IV. DISCUSSION

The major contribution of this study is the use of a Reynolds number (either Re_w or $\mathrm{Re}_{\mathrm{ISW}}$) to classify collapsing and plunging breakers. Although Re or Re_w have been previously applied to investigate the boundary-layer separation under an ISW [30–32], this study appears to be the first to apply a Reynolds number for ISW breaker classification. We preferred $\mathrm{Re}_{\mathrm{ISW}}$ to Re_w in this study, because it leads to a simple nondimensional index that delineates collapsing and plunging breakers. The proposed classification should be used when the breaker type based on the S_w-S classification by AG falls in the collapsing or plunging regime.

Another new result obtained in this study is the confirmation that the effect of the specific density ratio ε_d on ISW breaker types is small. Although Michallet and Ivey [17] showed that mixing efficiency is insensitive to ε_d, its effect on ISW breaker types does not appear to have been investigated before. It should be noted that the results in Michallet and Ivey [17] and this study do not imply small effects of ε_d on the overall mass transport induced by ISW breaking. For a given (displacement) amplitude, ISW-induced currents are proportional to the wave speed c_0, and hence ${\varepsilon_d}^{1/2}$, so ε_d can affect isopycnal mass transport of water mass with intermediate density created by ISW breaking.

Previous studies suggest that there are potentially competing Reynolds-number effects on ISW breaker types. On one hand, Aghsaee *et al.* [32] showed that the boundary layer is more susceptible to separation at higher momentum-thickness Reynolds number, although their results are valid only for a laminar boundary layer over a flat bottom. On the other hand, based on numerical simulations at relatively low and very high grid resolutions, AG argued that collapsing breakers, triggered by boundary layer separation, are less likely to occur at higher Re_w, because of smaller vortices resulting from the separation and slower growth of the instability. Our analysis of Reynolds-number effects is based on simulations at relatively low grid resolution [Figs. 6(b) and 6(c)], but the results are consistent with the high-resolution simulation by AG and collapsing is less likely to occur at higher Reynolds number.

It should be noted that the proposed classification has several caveats. One of them is that broad-crested ISWs ($A \approx (h_2 - h_1)/2$ when $\rho_1 \approx \rho_2$) are outside of the parameter range, because they were not considered in the experiments in BG, AG, and this study when $\rho_1 \approx \rho_2$. However, this is not of significant concern because the majority of observed ISWs are narrow-crested (see

Ref. [19], their Fig. 2). The second caveat is the use of two-dimensional numerical simulations, which do not capture three-dimensional processes such as secondary instability and subsequent mixing [51,60]. Since the focus of this study is the processes up to incipient ISW breaking, the use of two-dimensional model is considered sufficient for simulating initial two-dimensional instability [19,51,52]. The last caveat is that the breaker type, and hence proposed threshold between collapsing and plunging breakers in Eq. (12), will be modified if the no-slip bottom boundary is not resolved with the grid resolution employed in the numerical experiments [19]. The processes leading to fission, plunging, and surging are not very sensitive to grid resolution because they depend on kinematic and "adiabatic" processes. However, boundary-layer separation and ensuing instability, which causes collapsing, is more sensitive to grid resolution. Nonetheless, it is encouraging that the simulations in this study, and in AG, independently satisfy the proposed classification, suggesting that the results are relatively robust to differences in model formulation and simulation conditions. The resolution dependence of the threshold in Eq. (12) does not affect the result that the Reynolds number is a major factor in delineating collapsing and plunging breakers.

The proposed nondimensional index B_{ISW} can be calculated by including the effect of thickness of the pycnocline. Therefore, we need to test whether the proposed classification is applicable to these conditions. Background shear would also be an important factor [61], and its effects can be included in the calculation of c_0, α, and β [62]; however, this is beyond the scope of the present work. An eddy viscosity can also be used as ν to calculate $\mathrm{Re}_{\mathrm{ISW}}$. It remains to be investigated, in future work, which choice provides better classification of ISW breakers in the case including the effect of thickness of the pycnocline.

As an example application of the proposed classification, we apply Eq. (12) (with α instead of L_{SC}) to the numerical simulation in Vlasenko and Hutter [23]; although the grid resolution might be too coarse to resolve the no-slip bottom boundary layer in their simulation [19]. They simulated plunging to occur under the following conditions: $h_1 = 50\,\mathrm{m}$, $h_2 = 950\,\mathrm{m}$, $L = 18.8\,\mathrm{km}$, $L_{SC} = 17.8\,\mathrm{km}$, $\varepsilon_d = 0.00498$, $\nu \approx 0.001\,\mathrm{m^2\,s^{-1}}$, $\lambda \approx 500\,\mathrm{m}$, and $A = 84.4\,\mathrm{m}$. Since $S_w = 0.17$ and $S = 0.051$, this case is located in the collapsing or plunging regime in the $S_w - S$ classification (Fig. 5). The proposed classification does indicate a plunging breaker with $\mathrm{Re}_{\mathrm{ISW}} = 1.9 \times 10^5$, $S/S_w = 0.30$, and $B_{\mathrm{ISW}} = 7.3 \times 10^{11}$ [Fig. 6(c)].

V. CONCLUSIONS

This study investigated the classification of ISW breakers over a uniform slope in a two-layer stratified fluid based on present numerical experiments and previous laboratory [38] and numerical [19] experiments. We showed that the latest classification [19] based on the wave slope S_w and the bottom slope S does not classify collapsing and plunging ISW breakers in the published data sets, and that the use of S/S_w and a wave Reynolds number (either Re_w or $\mathrm{Re}_{\mathrm{ISW}}$) enables us to delineate them, with $\mathrm{Re}_{\mathrm{ISW}}$ being preferred as it requires a single equation. We proposed a nondimensional index $B_{\mathrm{ISW}} = (S/S_w)\mathrm{Re}_{\mathrm{ISW}}{}^2$ for the classification, with a threshold value (7×10^6). The applicability of the proposed classification to the case with the effect of thickness of the pycnocline remains to be investigated in the future.

ACKNOWLEDGMENTS

This work was supported by the Japan Society for the Promotion of Science under Grants No. 18H01545 and No. 18KK0119. This work was also supported in part by the Collaborative Research Program of Research Institute for Applied Mechanics, Kyushu University, and Research Center for Urban Safety and Security, Kobe University. K. Nakayama designed the all numerical computations and wrote most of the paper and performed all analysis. T. Sato performed the all numerical computations. K. Shimizu and L. Boegman discussed the analysis with K. Nakayama.

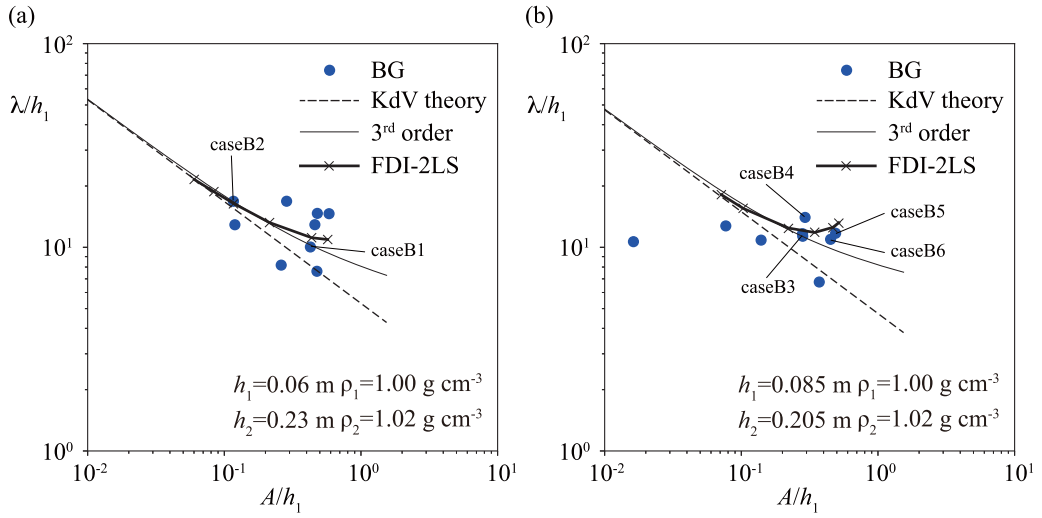

FIG. 8. Comparisons of amplitude–wavelength relationships. Cases with (a) $h_1 \approx 0.06$ m and (b) $h_1 \approx 0.085$ m from Boegman *et al.* [38].

APPENDIX

In this Appendix, we investigate whether the leading high-frequency internal wave in the laboratory experiments in BG can be considered as an ISW. They investigated the breaking of shoaling high-frequency internal waves formed by the degeneration of an internal seiche in a tilting tank. Since it takes a steepening timescale to form ISWs from an internal seiche [63,64], an ISW is formed only if this steepening timescale is shorter than the time it takes for the wave to break (see Fig. 7 in BG). To see if the leading high-frequency internal wave over the flat-bottom section was an ISW before reaching the uniform-slope section, we followed previous studies [55,65,66], and compared the experimental and theoretical amplitude–wavelength relationships over a flat bottom. To calculate the theoretical relationships for ISWs, we used the Fully nonlinear and strongly dispersive Internal wave equation in a two-layer system (FDI-2s) [54,67,68], because the third-order solution underestimates the wavelengths of large-amplitude ISWs (Fig. 8).

Since the ISWs were formed from an internal seiche, it is expected that background current affected the profiles of ISWs. For example, for surface waves in stratified fluids, background shear can increase the wavelength by more than 10% when the modified Froude number is larger than 1.0 [69–72]. Although the modified internal Froude number, including the effect of background current, is less than 1.0 in Boegman *et al.* [38], it should be noted that a wavelength might be overestimated slightly.

Based on the comparisons shown in Fig. 8, we used two and four cases from the cases with upper-layer thickness $h_1 \approx 0.06$ m and ≈ 0.085 m, respectively, in our analysis (Table II).

[1] K. G. Lamb, Internal wave breaking and dissipation mechanisms on the continental slope/shelf, Annu. Rev. Fluid Mech. **46**, 231 (2014).

[2] D. C. Pierson and G. A. Weyhenmeyer, High resolution measurements of sediment resuspension above an accumulation bottom in a stratified lake, Hydrobiologia **284**, 43 (1994).

[3] B. Steinman, W. Eckert, S. Kaganowsky, and T. Zohary, Seiche-induced resuspension in Lake Kinneret: A fluorescent tracer experiment, Water Air Soil Poll. **99**, 123 (1997).

[4] A. Wüest and A. Lorke, Small-scale hydrodynamics in lakes, Annu. Rev. Fluid Mech. **35**, 373 (2003).
[5] H. Sandstrom and J. A. Elliott, Internal tide and solitons on the Scotian Shelf: A nutrient pump at work, J. Geophys. Res. **89**, 6415 (1984).
[6] M. M. Omand, J. J. Leichter, P. J. Franks, R. T. Guza, A. J. Lucas, and F. Feddersen, Physical and biological processes underlying the sudden appearance of a red-tide surface patch in the nearshore, Limnol. Oceanogr. **56**, 787 (2011).
[7] E. McPhee-Shaw and E. Kunze, Boundary layer intrusions from a sloping bottom: A mechanism for generating intermediate nepheloid layers, J. Geophys. Res. **107**, 3050 (2002).
[8] K. Nakayama and J. Imberger, Residual circulation due to internal waves shoaling on a slope, Limnol. Oceanogr. **55**, 1009 (2010).
[9] K. Nakayama, T. Shintani, K. Kokubo, T. Kakinuma, Y. Maruya, K. Komai, and T. Okada, Residual current over a uniform slope due to breaking of internal waves in a two-layer system, J. Geophys. Res. **117**, C10002 (2012).
[10] M. Gloor, A. Wüest, and M. Münnich, Benthic boundary mixing and resuspension induced by internal seiches, Hydrobiologia **284**, 59 (1994).
[11] M. E. Inall, Internal wave induced dispersion and mixing on a sloping boundary, Geophys. Res. Lett. **36**, L05604 (2009).
[12] D. Bourgault, M. Morsilli, C. Richards, U. Neumeier, and D. E. Kelley, Sediment resuspension and nepheloid layers induced by long internal solitary waves shoaling orthogonally on uniform slopes, Cont. Shelf Res. **72**, 21 (2014).
[13] J. Pineda, Internal tidal bores in the nearshore: Warm-water fronts, seaward gravity currents and the onshore transport of neustonic larvae, J. Mar. Res. **52**, 427 (1994).
[14] P. Hosegood, J. Bonnin, and H. van Haren, Solibore-induced sediment resuspension in the Faeroe-Shetland Channel, Geophys. Res. Lett. **31**, L09301 (2004).
[15] L. Boegman and G. N. Ivey, Flow separation and resuspension beneath shoaling nonlinear internal waves, J. Geophys. Res. **114**, C02018 (2009).
[16] P. Aghsaee and L. Boegman, Experimental investigation of sediment resuspension beneath internal solitary waves of depression, J. Geophys. Res. **120**, 3301 (2015).
[17] H. Michallet and G. N. Ivey, Experiments on mixing due to internal solitary waves breaking on uniform slopes, J. Geophys. Res. **104**, 13467 (1999).
[18] J. Grue, A. Jensen, P. Rusas, and J. K. Sveen, Breaking and broadening of internal solitary waves, J. Fluid Mech. **413**, 181 (2000).
[19] P. Aghsaee, L. Boegman, and K. G. Lamb, Breaking of shoaling internal solitary waves, J. Fluid Mech. **659**, 289 (2010).
[20] M. H. Orr and P. C. Mignerey, Nonlinear internal waves in the South China Sea: Observation of the conversion of depression internal waves to elevation internal waves, J. Geophys. Res. **108**, 3064 (2003).
[21] E. L. Shroyer, J. N. Moum, and J. D. Nash, Observations of polarity reversal in shoaling nonlinear internal waves, J. Phys. Oceanogr. **39**, 691 (2009).
[22] R. Grimshaw, E. Pelinovsky, and T. Talipova, Solitary wave transformation due to a change in polarity, Stud. Appl. Math. **101**, 357 (1998).
[23] V. Vlasenko and K. Hutter, Numerical experiments on the breaking of solitary internal waves over a slope-shelf topography, J. Phys. Oceanogr. **32**, 1779 (2002).
[24] J. N. Moum, D. M. Farmer, W. D. Smyth, L. Armi, and S. Vagle, Structure and generation of turbulence at interfaces strained by internal solitary waves propagating shoreward over the continental shelf, J. Phys. Oceanogr. **33**, 2093 (2003).
[25] D. Fructus, M. Carr, J. Grue, A. Jensen, and P. A. Davies, Shear-induced breaking of large internal solitary waves, J. Fluid Mech. **620**, 1 (2009).
[26] K. G. Lamb and D. Farmer, Instabilities in an internal solitary-like wave on the Oregon Shelf, J. Phys. Oceanogr. **41**, 67 (2011).
[27] H. van Haren, M. Ribó, and P. Puig, (Sub-)inertial wave boundary turbulence in the Gulf of Valencia, J. Geophys. Res. **118**, 2067 (2013).

[28] D. Bogucki, T. Dickey, and L. G. Redekopp, Sediment resuspension and mixing by resonantly generated internal solitary waves, J. Phys. Oceanogr. **27**, 1181 (1997).
[29] D. Bogucki and L. G. Redekopp, A mechanism for sediment resuspension by internal solitary waves, Geophys. Res. Lett. **26**, 1317 (1999).
[30] P. J. Diamessis and L. G. Redekopp, Numerical investigation of solitary internal wave-induced global instability in shallow water benthic boundary layers, J. Phys. Oceanogr. **36**, 784 (2006).
[31] M. Carr, P. A. Davies, and P. Shivaram, Experimental evidence of internal solitary wave-induced global instability in shallow water benthic boundary layers, Phys. Fluids **20**, 066603 (2008).
[32] P. Aghsaee, L. Boegman, P. J. Diamessis, and K. G. Lamb, Boundary-layer-separation-driven vortex shedding beneath internal solitary waves of depression, J. Fluid Mech. **690**, 321 (2012).
[33] K. G. Lamb, A numerical investigation of solitary internal waves with trapped cores formed via shoaling, J. Fluid Mech. **451**, 109 (2002).
[34] B. C. Wallace and D. L. Wilkinson, Run-up of internal waves on a gentle slope in a two-layered system, J. Fluid Mech. **191**, 419 (1988).
[35] K. R. Helfrich, Internal solitary wave breaking and run-up on a uniform slope, J. Fluid Mech. **243**, 133 (1992).
[36] A. Scotti and J. Pineda, Observation of very large and steep internal waves of elevation near the Massachusetts coast, Geophys. Res. Lett. **31**, L22307 (2004).
[37] S. K. Venayagamoorthy and O. B. Fringer, On the formation and propagation of nonlinear internal boluses across a shelf break, J. Fluid Mech. **577**, 137 (2007).
[38] L. Boegman, G. N. Ivey, and J. Imberger, The degeneration of internal waves in lakes with sloping topography, Limnol. Oceanogr. **50**, 1620 (2005).
[39] C. J. Galvin, Breaker type classification on three laboratory beaches, J. Geophys. Res. **73**, 3651 (1968).
[40] J. A. Battjes, Surf similarity, in *Proceedings of the 14th International Conference on Coastal Engineering* (American Society of Civil Engineers, Copenhagen, Denmark 1974), pp. 466–480.
[41] Y. Goda, *Random Seas and Design of Maritime Structures*, 3rd ed. (World Scientific, Singapore, 2010), p. 213.
[42] G. Forgia, T. Tokyay, C. Adduce and G. Constantinescu, Numerical investigation of breaking internal solitary waves, Phys. Rev. Fluids. **3**, 104801 (2018).
[43] B. R. Sutherland, K. J. Barrett, and G. N. Ivey, Shoaling internal solitary waves, J. Geophys. Res. **118**, 4111 (2013).
[44] Y. Maruya, K. Nakayama, T. Shintani, and M. Yonemoto, Evaluation of entrainment velocity induced by wind stress in a two-layer system, Hydrol. Res. Lett. **4**, 70 (2010).
[45] A. Nakamoto, K. Nakayama, T. Shintani, Y. Maruya, K. Komai, T. Ishida, and Y. Makiguchi, Adaptive management in Kushiro Wetland in the context of salt wedge intrusion due to sea level rise, Hydrol. Res. Lett. **7**, 1 (2013).
[46] K. Nakayama, T. Shintani, K. Shimizu, T. Okada, H. Hinata, and K. Komai, Horizontal and residual circulations driven by wind stress curl in Tokyo Bay, J. Geophys. Res. **119**, 1977 (2014).
[47] K. Nakayama, H. D. Nguyen, T. Shintani, and K. Komai, Reversal of secondary circulations in a sharp channel bend, Coast. Eng. J. **58**, 1650002 (2016).
[48] A. J. Adcroft, C. N. Hill, and J. Marshall, Representation of topography by shaved cells in a height coordinate ocean model, Mon. Wea. Rev. **125**, 2293 (1997).
[49] W. P. Jones and B. E. Launder, The prediction of laminarization with a two-equation model of turbulence, Int. J. Heat Mass Transfer **15**, 301 (1972).
[50] L. Umlauf and H. Burchard, A generic length-scale equation for geophysical turbulence models, J. Mar. Res. **61**, 235 (2003).
[51] O. B. Fringer and R. L. Street, The dynamics of breaking progressive interfacial waves, J. Fluid Mech. **494**, 319 (2003).
[52] D. Bourgault and D. E. Kelly, On the reflection of uniform slopes for normally incident internal solitary waves, J. Phys. Oceanogr. **37**, 1156 (2007).
[53] R. M. Mirie and S. A. Pennell, Internal solitary waves in a two-fluid system, Phys. Fluids A **1**, 986 (1989).

[54] K. Nakayama, T. Kakinuma, M. Oikawa, H. Tsuji, and Y. Maruya, Applicability of third-order theoretical solutions into internal waves, J. JSCE Ser. B2 Coast. Eng. **57**, 171 (2010) (in Japanese with English abstract).
[55] C. G. Koop and G. Butler, An investigation of internal solitary waves in a two-fluid system, J. Fluid Mech. **112**, 225 (1981).
[56] B. M. Sumer, P. M. Jensen, L. B. Sørensen, J. Fredsøe, P. L.-F. Liu, and S. Carstensen, Coherent structures in wave boundary layers. Part 2. Solitary motion, J. Fluid Mech. **646**, 207 (2010).
[57] G. Vittori and P. Blondeaux, Characteristics of the boundary layer at the bottom of a solitary wave, Coastal Eng. **58**, 206 (2011).
[58] C. E. Ozdemir, T.-J. Hsu, and S. Balachandar, Direct numerical simulations of instability and boundary layer turbulence under a solitary wave, J. Fluid Mech. **731**, 545 (2013).
[59] P. E. Holloway, Internal hydraulic jumps and solitons at a shelf break region on the Australian North West Shelf, J. Geophys. Res. **92**, 5405 (1987).
[60] R. S. Arthur and O. B. Fringer, The dynamics of breaking internal solitary waves on slopes, J. Fluid Mech. **761**, 360 (2014).
[61] M. Stastna and K. G. Lamb, Vortex shedding and sediment resuspension associated with the interaction of an internal solitary wave and the bottom boundary layer, Geophys. Res. Lett. **29**, 1512 (2002).
[62] R. Grimshaw, E. Pelinovsky, and O. Poloukhina, Higher-order Korteweg-de Vries models for internal solitary waves in a stratified shear flow with a free surface, Nonlin. Proc. Geophys. **9**, 221 (2002).
[63] D. A. Horn, L. G. Redekopp, J. Imberger, and G. N. Ivey, Internal wave evolution in a space-time varying field, J. Fluid Mech. **424**, 279 (2000).
[64] D. A. Horn, J. Imberger, G. N. Ivey, and L. G. Redekopp, A weakly nonlinear model of long internal waves in closed basins, J. Fluid Mech. **467**, 269 (2002).
[65] J. Grue, H. A. Friis, E. Palm, and P. O. Rusas, A method for computing unsteady fully nonlinear interfacial waves, J. Fluid Mech. **351**, 223 (1997).
[66] W. Choi and R. Camassa, Fully nonlinear internal waves in a two-fluid system, J. Fluid Mech. **396**, 1 (1999).
[67] K. Nakayama and T. Kakinuma, Internal waves in a two-layer system using fully nonlinear internal-wave equations, Int. J. Num. Method. Fluids **62**, 574 (2010).
[68] K. Nakayama, T. Kakinuma, and H. Tsuji, Oblique reflection of large internal solitary waves in a two-layer fluid, European Journal of Mechanics - B/Fluids **74**, 81 (2018).
[69] R. A. Dalrymple, A finite amplitude wave on a linear shear current, J. Geophys. Res. **79**, 4498 (1974).
[70] J. M. Vanden-Broeck, Steep solitary waves in water of finite depth with constant vorticity, J. Fluid Mech. **274**, 339 (1994).
[71] A. F. Teles da Silva and D. Peregrine, Steep steady surface waves on water of finite depth with constant vorticity, J. Fluid Mech. **195**, 281 (1988).
[72] W. Choi, Strongly nonlinear long gravity waves in uniform shear flows, Phys. Rev. E **68**, 026305 (2003).